

# Direct demonstration of circulating currents in a controllable $\pi$ -SQUID generated by a 0 to $\pi$ transition of the weak links.

J.J.A. Baselmans, B.J. van Wees, and T.M. Klapwijk \*  
*Department of Applied Physics and Materials Science Center,  
 University of Groningen,  
 Nijenborg 4, 9747 AG Groningen, The Netherlands*  
 \* *Department of Applied Physics and DIMES,  
 Delft University of Technology,  
 Lorentzweg 1, 2628 CJ Delft, The Netherlands*

(Dated: February 1, 2008)

A controllable  $\pi$ -SQUID is a DC SQUID with two controllable  $\pi$ -junctions as weak links. A controllable  $\pi$ -junction consists of a superconducting - normal metal - superconducting Josephson junction with two additional contacts to the normal region of the junction. By applying a voltage  $V_c$  over these contacts it is possible to control the state of the junction, i.e. a conventional (0) state or a  $\pi$ -state, depending on the magnitude of  $V_c$ . We demonstrate experimentally that, by putting one junction into a  $\pi$ -state, a screening current is generated around the SQUID loop at integer external flux. To be able to do this, we have fabricated controllable  $\pi$ -junctions, based on Cu-Nb or Ag-Nb, in a new geometry. We show that at 1.4 K only the Nb-Ag device shows the transition to a  $\pi$ -state as a function of  $V_c$  consistent with theoretical predictions. In a controllable  $\pi$  SQUID based on Nb-Ag we observe, a part from a screening current at integer external flux, a phase shift of  $\pi$  of the  $V_{SQUID} - B$  oscillations under suitable current bias, depending on the magnitude of  $V_c$ .

PACS numbers:

## I. INTRODUCTION

In recent years considerable attention has been paid to controllable Josephson junctions. In general, such a Josephson junction consists of a Superconductor-normal metal-superconductor (SNS) junction with additional electrodes connected to the normal region of the junction. Inside the normal region coherent quantum states are formed due to the presence of the two superconducting electrodes. The properties of the junction, and in particular the critical current  $I_c$  are determined by the energy spectrum *and* the occupation of these states. Hence it is possible to change  $I_c$  by changing the energy distribution of the quasiparticles in the junction normal region<sup>1,2,3,4,5</sup>. This is done by sending a control current through the additional electrodes connected to the normal region or by applying a control voltage  $V_c$  over them. Several experiments have been performed the past years on these devices, which differ mainly in the way in which the energy of the quasiparticles is changed<sup>6,7,8,9,10</sup>. The most interesting situation is that of the so called controllable  $\pi$ -junctions<sup>9,10</sup>. In these systems it is not only possible to change the magnitude of the critical current of the junction but also to reverse its direction with respect to the phase difference  $\varphi$  between the two superconducting electrodes. This sign reversal is equivalent to the introduction of an extra phase factor  $\pi$  in the Josephson supercurrent ( $I_{sc}$ )-phase relation

$$I_{sc} = I_c \sin(\varphi) \Rightarrow I_{sc} = -I_c \sin(\varphi) \equiv I_c \sin(\varphi + \pi) \quad (1)$$

This means that for zero supercurrent, the ground state is that of a macroscopic phase difference equal

to  $\pi$ . There is an analogy here with  $\pi$ -junctions associated with bi-crystals<sup>11</sup> or 's-d' contacts in ceramic superconductors<sup>12</sup> and  $\pi$ -junctions using a dilute ferromagnet f' as the "normal" region of a S-f'-S junction<sup>13,14</sup>. However, the ceramic systems remain a  $\pi$ -junction (or normal junction) once fabricated and the S-f'-S junctions switch between a normal and a  $\pi$ -state only as a function of temperature. This in contrast with the controllable  $\pi$ -junction where the state of the junction as well as the magnitude of the critical current is fully controllable by means of the control voltage.

Using such controllable  $\pi$ -junctions as weak links of a DC SQUID (direct current superconducting quantum interference device), it is possible to tune the critical currents of the individual weak links. More interestingly, it is possible to add an extra phase of  $\pi$  or  $2\pi$  to the SQUID loop without the application of an external magnetic field by switching one or two of the junctions in a  $\pi$  state. An extra phase factor of  $\pi$  is identical to the external application of half a flux quantum,  $\phi_0/2$ , with  $\phi_0 = 2.07 \cdot 10^{-7}$  Wb. This is a direct consequence of the condition of a single-valued wave function around the SQUID loop,

$$\frac{2\pi\phi}{\phi_0} - \varphi_1 - \varphi_2 = 2\pi n \quad , \quad (2)$$

where  $\phi$  is the total flux in the ring,  $n$  is an integer and  $\varphi_1$  and  $\varphi_2$  are the phases over the two Josephson junctions, as shown in Fig.1a. Switching one junction in the  $\pi$ -state at an external flux  $\phi = n\phi_0$  adds  $\pi$  to the left hand side of Eq.2. This leads to the same solution of the equation if the junction would be in the "conventional"

state with an external flux  $\phi = (n \pm \frac{1}{2})\phi_0$ . Hence it is possible to generate a screening current in a SQUID with a sufficiently large inductance in the absence of a magnetic field.

The main purpose of this paper is to demonstrate unequivocally that it is possible to add a macroscopic quantum phase of  $\pi$  or  $2\pi$  to a DC SQUID with 2 controllable  $\pi$ -junctions as weak links. We demonstrate that this results in a screening current that can be switched on or off depending on  $V_c$  at an external flux of an integer flux quantum.

The outline is the following: We begin, in section II, with a very short description of the basics of the DC SQUID and a description of the theoretical concepts regarding controllable  $\pi$ -junctions. In section III we discuss the sample design and fabrication and in section IV we discuss experiments on single controllable  $\pi$ -junctions made of Nb-Ag or Nb-Cu. The geometry of these devices differs from the conventional cross shape. We show that the Nb-Ag device shows a  $0$  to  $\pi$  transition at 1.4 K, in contrast with the Nb-Cu device. The full dependence of the critical currents of both devices on  $V_c$  is in good quantitative agreement with the theoretical predictions discussed in section II. In section V we proceed with measurements on a controllable SQUID, made of Ag-Nb. We show that the magnitude and sign of the voltage oscillations of the SQUID as a function of the magnetic field under suitable current bias can be tuned. In the last section we measure directly the flux expelled by the screening current in a controllable SQUID by placing a smaller SQUID directly behind it. We show that the screening current around integer external flux can be switched on or off by switching one of the junctions of the controllable SQUID in a  $\pi$ - or a normal state.

## II. THEORETICAL CONCEPTS

### A. the DC SQUID

Before we discuss the controllable  $\pi$ -junction it may be helpful to discuss the basics of the DC SQUID<sup>15,16,17</sup>. A DC SQUID is a ring of superconducting material with self inductance  $L$  and two Josephson junctions with a critical currents  $I_{c1}$  and  $I_{c2}$ . In the absence of any external flux,  $\phi_{ext}$ , the SQUID is in equilibrium and behaves as a single Josephson junction with a total critical current  $I_c = I_{c1} + I_{c2}$ . If  $\phi_{ext} \neq 0$ , then the total flux  $\phi$  in the SQUID loop changes, depending on its self inductance, according to

$$\phi = \phi_{ext} + LJ \quad , \quad (3)$$

with  $J$  the screening current running around the SQUID loop. The flux in the loop,  $\phi$ , also depends on the phases

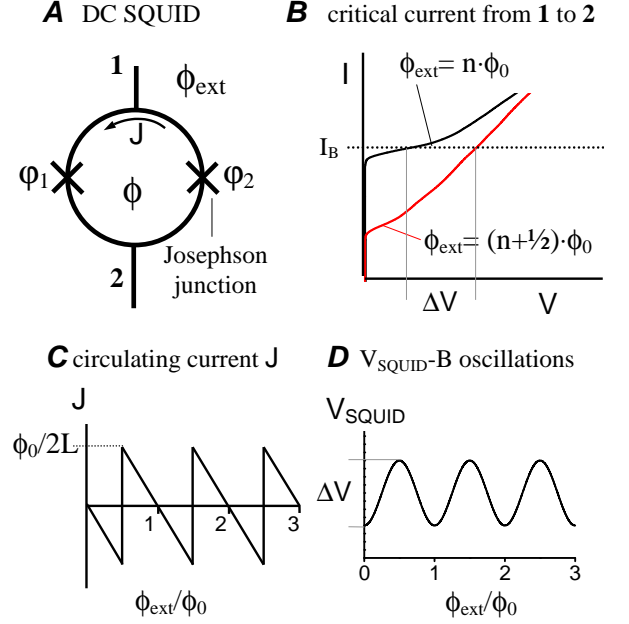


FIG. 1: Basic operation of the DC SQUID. (A) shows a DC SQUID with a screening current  $J$  due to an external flux  $\phi_{ext}$ . The supercurrent of the SQUID, as shown in (B), oscillates as a function of  $\phi_{ext}$ . By applying a current bias  $I_B$  the oscillating critical current is transferred into an oscillating voltage  $V_{SQUID}$  between contacts 1 and 2 (A), as shown in (D). The screening current  $J$  has, in the limit of large self inductance  $L$ , a saw tooth shape as a function of  $\phi_0$ , as shown in (C).

of the two Josephson junctions

$$\varphi_1 = \frac{2\pi\phi}{\phi_0} - \varphi_2 \quad , \quad (4)$$

which is directly obtained from Eq.2. In the limit of small self inductance, so that the  $LJ$  term in Eq.3 is negligible and if  $I_{c1} = I_{c2} \equiv I_{c1,2}$ , it is easy to show that

$$I_c = 2I_{c1,2} \left| \cos \left( \frac{2\pi\phi_{ext}}{\phi_0} \right) \right| \quad , \quad (5)$$

where we use Eqs.1,3 and 4. In this case  $I_c$  is periodic in  $\phi_0$  and varies between  $2I_{c1,2}$  at  $\phi_{ext} = n\phi_0$  and 0 at  $\phi_{ext} = (n + 1/2)\phi_0$ . At nonzero inductance the periodicity remains the same but the amplitude of the  $I_c$  modulation is reduced, for  $I_c=0$  is not reached at  $\phi = \pi/2$  due to the presence of the circulating current  $J$ . In the limit of large self inductance, the amplitude of the  $I_c$  modulation decreases to  $\phi_0/L$ , whereas  $J$  becomes a saw tooth function varying linearly from  $-\phi_0/2L$  to  $+\phi_0/2L$ , as shown in Fig.1(B) and (C). The periodic behavior of  $I_c$  as function of  $\phi_{ext}$  can be transformed into a periodic voltage by sending a bias current  $I_B$  a little larger than the maximum value of  $I_c$  through the SQUID. Due to the non-linear I-V curve of the SQUID the difference in  $I_c(\phi_{ext})$  translates into a voltage  $V_{SQUID}(\phi_{ext})$ , thus cre-

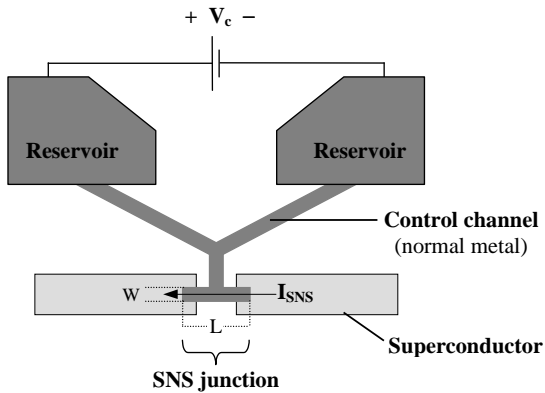


FIG. 2: Schematic drawing of a controllable  $\pi$ -junction. The center of the control channel, which connects two large reservoirs, is coupled to the normal region of a co-planar SNS junction. By applying a voltage  $V_c$  over the reservoirs the energy distribution of the quasiparticles in the channel and hence in the normal region of the SNS junction is changed. As a result the occupation of the supercurrent carrying states in N is changed, resulting in a change in the critical value of the supercurrent  $I_{SNS}$ .

ating a very sensitive flux to voltage transformer. The resulting  $V_{SQUID} - B$  oscillations are shown in Fig.1(D).

### B. Controllable $\pi$ -junctions

A controllable  $\pi$ -junctions is a device that combines two different structures in one: A thin film SNS junction and a short mesoscopic wire (which we call control channel) between two large electron reservoirs in thermal equilibrium. A schematic drawing is given in Fig.2: The center of the control channel, which connects two large reservoirs, is coupled to the normal region of a co-planar thin film SNS junction, in which the normal region partly overlaps the superconducting electrodes. The length and width of the normal region are denoted by  $L$  and  $w$  in the figure. The size of the junction  $L \lesssim 1\mu m$  and the control channel length,  $l \sim 5\mu m$ , is larger than the elastic mean free path of the electrons, which is approximately given by the film thickness ( $\sim 50nm$ ). Hence the electron motion is diffusive.

The principle of operation is the following: The presence of the two superconducting electrodes induces a continuous spectrum of supercurrent carrying states  $Im(J(E))$  in the normal region of the junction, which is responsible for the supercurrent transport ( $I_{SNS}$  in Fig.2). The energy scale  $E$  is the energy with respect to the Fermi level. As stated before, the critical value of  $I_{SNS}$ ,  $I_c$ , is determined by the energy spectrum and the occupation of these supercurrent carrying states. The occupation of the states is determined by the energy distribution of the quasiparticles in the normal

region of the junction,  $f(E)$ , which is identical to the energy distribution in the center of the control channel. This energy distribution can be modified by means of applying a voltage  $V_c$  over the control channel, so  $f(E) = f(E, V_c)$ . The relation between  $I_c$ ,  $Im(J(E))$  and  $f(E, V_c)$  is given by<sup>1,2,3,4,5</sup>:

$$I_c = \frac{1}{R_n} \int_{-\infty}^{\infty} dE [1 - 2f(E, V_c)] Im(J(E, \varphi = \pi/2)), \quad (6)$$

where  $\varphi$  the phase difference between the superconducting electrodes<sup>18</sup>. It is important to realize that the critical current is modified by changing the energy of the quasiparticles in the normal region and not by the flow of the control current associated with  $V_c$ . In the present geometry this is quite clear, because the current paths of  $I_{SNS}$  and the control current are separated. This is in contrast with the conventional cross geometry, where  $I_{SNS}$  crosses the control current. However, even in this case it is the energy of the quasiparticles and not the control current that determines the critical current.

To calculate the dependence of  $I_c$  as a function of  $V_c$  we need to know both the shape of the supercurrent carrying density of states,  $Im(J(E))$  and the shape of the quasiparticle energy distribution in the normal region of the junction,  $f(E, V_c)$ . The exact energy dependence of  $Im(J(E))$  is calculated using the quasi-classical Green's function theory<sup>1,2,3,4</sup>. It depends on the ratio of the Thouless energy with the energy gap  $\Delta$  of the superconductors. The Thouless energy is given by  $E_{th} = \hbar D/L^2$ , with  $L$  the length of the normal region of the SNS junction<sup>19</sup> and  $D$  the diffusion constant of the normal metal. The general shape of  $Im(J(E))$ , as shown by the solid black line in both panels of Fig. 3 is a strongly damped oscillation with a hard gap at low energies  $E \lesssim E_{th}$ . The positive and negative parts of the supercurrent carrying density of states represent energy dependent contributions to the supercurrent in the positive and negative direction.

The other relevant quantity of the system is the quasiparticle energy distribution,  $f(E, V_c)$ . The exact shape of  $f(E, V_c)$  in the center of the control channel (and hence in the junction normal region) depends, as shown by Pothier *et al.*<sup>20</sup>, on the voltage  $V_c$  applied over the control channel and on the amount of electron-electron and electron-phonon scattering. At low temperatures,  $T \lesssim 1K$ , electron-electron scattering is the dominant relaxation mechanism and the electron energy distribution depends only on  $V_c$  and the electron-electron interaction. In this case, we can distinguish two limiting possibilities:

1: *no electron-electron interaction* If the control channel is sufficiently short, so that the electron-electron interaction time  $\tau_0$  exceeds the diffusion time  $\tau_D$  through the channel, the electrons conserve their energy. The resulting electron energy distribution in the center of

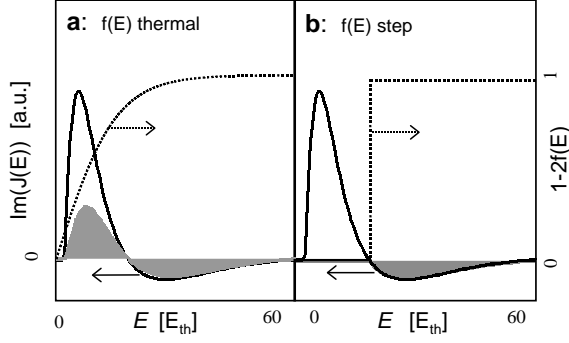


FIG. 3: Supercurrent carrying density of states  $Im(J(E))$  for  $\Delta/E_{th}=70$  at  $\varphi = \pi/2$  (solid line) together with  $1 - 2f(E)$  (dotted line) in the case of a thermal distribution (a), and a step distribution (b). The shaded area represents the contributions to the integrand of Eq.6.  $E$  represents the energy with respect to the Fermi level  $E_{th}$  is the Thouless energy.

the wire is given by<sup>20</sup>

$$f(E, V_c) = 1/2 \cdot \left[ f_d \left( E - \frac{eV_c}{2} \right) + f_d \left( E + \frac{eV_c}{2} \right) \right], \quad (7)$$

here  $f_d(E)$  is the Fermi-Dirac distribution at a temperature  $T$

$$f_d(E) = \left[ 1 + \exp \left( \frac{E}{k_B T} \right) \right]^{-1}, \quad (8)$$

with  $k_B$  Boltzmann's constant. Eq.7 is the renormalized addition of the thermal distribution functions of the reservoirs with an energy separation of  $eV_c$ . This represents, if  $k_B T < eV_c$ , a double step structure with an occupation fraction of 1/2 in an energy range of  $eV_c$  around the Fermi energy. Such a step distribution will, at a large enough value of  $V_c$ , block all the positive contributions of  $Im(J(E))$ , as shown in Fig. 3b, because an occupation fraction of 1/2 causes the integrand of Eq.6 to vanish. This results in a reversal in the direction of the supercurrent and hence the transition to a  $\pi$ -state

**2: very strong electron-electron interaction** If the control channel is very long, so that  $\tau_0 \ll \tau_D$ , the electron system regains a *local* thermal equilibrium. The energy distribution given by the Fermi-Dirac distribution, with an effective temperature  $T_{eff} > T_{Bath}$ ,

$$T_{eff} = \sqrt{T_{bath}^2 + (aV_c)^2}. \quad (9)$$

Here  $T_{bath}$  is the bath temperature and  $a$  can be calculated using the Wiedemann-Franz law, resulting in  $a=3.2$  K/mV. This situation is called the 'hot electron limit'. The result, a Fermi-Dirac distribution with a width increasing with  $V_c$ , causes a rapid decay of the supercurrent, as shown in the left panel of Fig.3a

due to the compensation of the positive and negative contributions in  $Im(J(E))$ .

The shape of the distribution function in a real experiment is in general in between these two limits, with possible modifications due to electron-phonon interactions. We calculate the exact shape of the energy distribution function using a model presented by Pothier *et al.*<sup>20,21</sup>. In this model the shape of the electron energy distribution in the wire depends on four parameters: The voltage  $V_c$  applied over the wire, the effective strength of the electron - electron interaction, the effective strength of the electron phonon interaction and possible heating of the reservoirs. The electron-electron interaction is described by a two-particle interaction with an interaction Kernel  $K_\alpha \epsilon^{-\alpha} \cdot \tau_D$ . Here  $\epsilon$  is the energy transferred between two interacting particles and  $\tau_D$  the diffusion time through the wire. The magnitude  $K_\alpha$  and energy dependence  $\alpha$  of the electron - electron interaction can be calculated by means of a direct calculation of the screened Coulomb interaction in a homogenous 1-dimensional diffusive conductor<sup>24,25</sup>. Without going into detail it is important to realize that a direct measurement of the electron energy distribution function in diffusive 1D gold, copper and silver wires using tunnel junction spectroscopy<sup>20,21,22,23</sup> yields material dependent results for  $K_\alpha \epsilon^{-\alpha}$  which are not consistent with the theoretical predictions using refs.<sup>24,25</sup> alone. Because the control channels used in our experiment are similar to the wires measured in refs.<sup>20,21,22,23</sup>, we have used the experimental values of  $\alpha$  in our calculations:  $\alpha = 2$  for copper and  $\alpha = 1.2$  for Ag. The strength of the interaction,  $K_\alpha$  is used as a fit parameter.

In the model, the effect of electron-phonon scattering is implemented in a similar way. The magnitude of the interaction kernel is, in this case, deduced from measurements of the phase relaxation time<sup>26</sup>, and given by  $K_{phonon} = 8ns^{-1}meV^{-3}$  for Cu and Ag.

As a last input parameter, possible heating of the reservoirs should be taken into account. The power associated with the application of the control voltage,  $P = V_c^2/R_c$  ( $R_c$  is the control channel resistance) is injected into the reservoirs. At low bath temperatures ( $T < 1K$ ), low values of  $R_c$  and large values of  $V_c \gtrsim 1mV$ , the electron gas in the reservoirs can attain a much higher effective temperature than the bath temperature<sup>27,28</sup>. However, all experiments presented in the remainder of the text are performed at relatively high temperatures of 1.4 K, resulting in negligible heating of the reservoirs<sup>29</sup>.

### III. SAMPLE DESIGN AND FABRICATION

So far, all experimental evidence of a controllable  $\pi$ -junction<sup>9,10</sup> has been achieved using devices with a cross geometry. The control channel and the normal region of the junction are in fact a single cross shaped metallic wire, with superconducting contacts at the first two

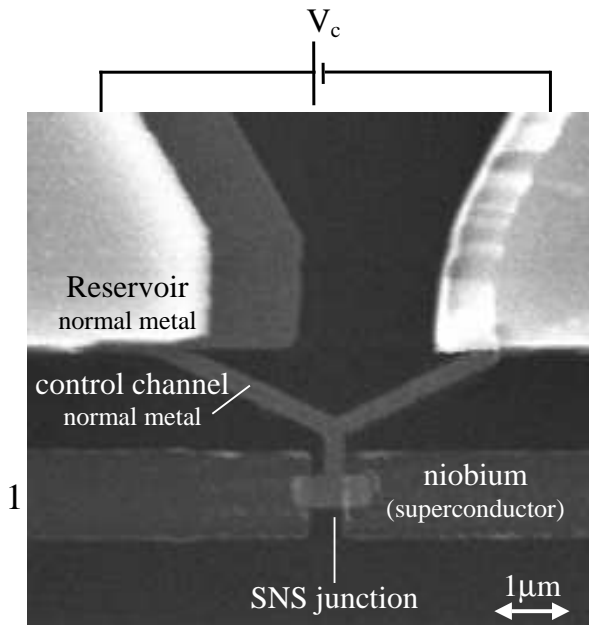


FIG. 4: Scanning electron micrograph of a controllable  $\pi$ -junction using side contacts. In this case the normal metal is silver, whereas also similar samples using copper are made.

opposite ends and large reservoirs at the others. This geometry is not suitable for use in a SQUID geometry, because one of the reservoirs of each junction would have to be within the SQUID loop, which is not possible due to the large reservoir sizes needed. Therefore we use a device geometry with side contacts (see Fig.4), such as used by Morpurgo *et al.*<sup>6</sup> in the thermal limit. The disadvantage of this geometry is that it imposes a larger minimum length on the control channel than the conventional cross geometry, where this length can be reduced to about  $1 \mu\text{m}$ . As a consequence, a material with a slow electron-electron relaxation is needed to be able to maintain a non-thermal energy distribution in the control channel. For this reason gold is unsuitable as the normal metal<sup>20,21,22,23,30</sup> and copper or preferably silver should be used.

We now describe the sample fabrication, referring to Fig. 4. The samples have been realized on a thermally oxidized Si wafer that is covered with a 150 nm layer of sputter deposited  $\text{Al}_2\text{O}_3$  to improve the adhesion of Ag and Cu. In the first step 50 nm of Nb is deposited using standard e-beam lithography, DC sputtering and subsequent lift-off. The critical temperature of the sputtered film is 8.1 K. Subsequently the normal region, control channel and the reservoirs (Ag or Cu) are deposited using shadow evaporation without breaking the vacuum. This is needed because the adhesion of these metals is poor, implying that it is not possible to bake a deposited film to be able to do another lithography step. We use a double layer of PMMA-MA and PMMA with e-beam lithography and wet etching to create a PMMA suspended mask.

TABLE I: Parameters of the single SNS junctions.  $R_n$  is the normal state resistance of the SNS junction,  $L$  is the length of the normal region and  $W$  the width (see Fig.2).  $E_{th}$  is the Thouless energy obtained using  $D$  and  $L$ .

sample	$L \times W$ [nm]	$R_n$ [ $\Omega$ ]	$D$ [ $\text{m}^2/\text{s}$ ]	$E_{th}$ [ $\mu\text{eV}$ ]
Ag	1000x400	0.65	0.023	14
Cu	800 x 600	0.8	0.021	21

The deposition of the metals is done in an UHV deposition system with a background pressure of  $5 \cdot 10^{-10}$  mBar, the pressure in the system during the evaporation steps is  $\leq 5 \cdot 10^{-8}$  mBar. Prior to deposition we use Argon etching ( $P_{Ar} = 1 \cdot 10^{-4}$  mBar, 500 V) for 3.5 minutes to clean the Nb surface. Subsequently we deposit, in the case of an Ag sample, 10 nm of Ti adhesion layer under a large angle ( $47^\circ$ , resulting in a shift to the left in the figure), with the result that the Ti layer is only deposited on the substrate at the position of the reservoirs and not at the position of the thin openings defining the control channel and the normal region of the junction. This is important, for the effect of a thin Ti layer upon the electron-electron interaction time is not known. Then we deposit 50 nm Ag perpendicular to the substrate, thus creating the control channel and the normal region of the junction. As a last step 700 nm of Ag is deposited again at  $47^\circ$  to form the reservoirs with an effective thickness of 475 nm. In Fig.4 the left shift due to the large evaporation angle of the reservoirs with respect to the control channel is clearly visible. A (parasitic) projection of the control channel and the normal region of the SNS junction is not present, because the aspect ratio of the top resist is so large for these structures that the metal is deposited into the side wall of the resist. This results in a removal of these projections during lift-off. The fabrication of the Cu samples is identical except for the fact that Cu is used for the normal conducting regions of the device and that no Ti adhesion layer is used underneath the reservoirs. We found that this is not necessary for sufficient adhesion. The length of the control channel cannot be made shorter, because the resist will become unstable if the large openings defining the reservoirs come any closer<sup>31</sup>. To measure the quality of the niobium - normal metal interface we have made, in every fabrication run, a cross of a 200 nm wide Nb and normal metal wire. The resistance of the 200x200 nm interface has been determined to be  $\approx 0.1 \Omega$  each time, which is smaller than the square resistance of the normal metal ( $0.4 \Omega$ ), indicating that the interface is clean.

#### IV. EXPERIMENTS ON SINGLE JUNCTIONS

In the experiment, performed at 1.4 K in a pumped He bath, we measure the critical current of the SNS junction (from contacts 1 to 2) as a function of the voltage  $V_c$  applied over the control channel (see Fig. 4). The mea-

TABLE II: Result of the fits on the single junctions. For  $\alpha$  we use the experimental values from Ref.<sup>20,21</sup>:  $\alpha=2$  for Cu and 1.2 for silver.

sample	$K_\alpha [ns^{-1}\mu eV^{\alpha-2}]$	$E_{th} [\mu eV]$	$\tau_D [ns]$
Ag	0.65	13	2.3
Cu	1.7	21.5	2.5

surement of the critical current consists of sweeping the bias current while measuring the differential resistance  $dV/dI$  using a small AC modulation on the bias current. We define the experimental critical current where the differential resistance reaches half its normal state value<sup>19</sup>. The control voltage is applied using another current source, with floating ground and  $V_c$  is measured by means of voltage probes close to the control channel ends (not visible in the figure). The measurement of  $V_c$  shows a slight modulation if the current bias through the SNS junction is smaller than the critical current, associated with Andreev interferometry<sup>32,33</sup>. This modulation is used to determine the state of the junction<sup>9</sup>. The experiment is performed on several devices made of Cu-Nb and Ag-Nb. All samples show identical behavior and we present the data of two samples, one made of Ag-Nb and one made of Cu-Nb. The exact parameters of these two samples are given in Table I. The experimental critical current as a function of  $V_c$  is shown by the solid circles in Fig. 5. From the figure is obvious that the Ag-Nb device shows a transition to a  $\pi$ -junction above  $V_c = V_{c,critical} = 430\mu V$  and that the device made of Cu-Nb does not show this transition. The magnitude of the equilibrium critical current at 1.4 K is, in the case of Ag, in good agreement theoretical predictions presented by Dubos *et al.*<sup>19</sup>. The measured fraction of  $I_c R_n / E_{th} = 0.44$ , whereas 0.5 is predicted. For the copper sample the agreement is less good. In this case we measure 0.5 whereas 2 is predicted. The next step in our analysis is a quantitative comparison of the experimental data with the theory. As input parameters to calculate the distribution function, we use, for  $\alpha$  and  $K_{phonons}$  the values given in section II<sup>20,21</sup>,  $K_{phonons} = 8 ns^{-1} meV^{-3}$ ,  $\alpha=1.2$  for Ag and 2 for Cu. As stated before, reservoir heating is negligible due to the relatively high bath temperature and large control channel resistances ( $\sim 8 \Omega$  for both samples), despite the large values of  $V_c$ ,<sup>29</sup>. Using  $E_{th}$  and  $K_{alpha}$  as fit parameters, we obtain the best fit, as shown by the black lines in both panels of Fig.5, using the parameters shown in Table II. In the Table, we have calculated  $\tau_D = \frac{l^2}{D}$  using for  $l$  the total diffusion length, given by the length of the v-shaped wire plus two times the T-shaped extension towards the junction, yielding  $l=5+2\cdot 1=7\mu m$  (see Fig.4. The fits are very good over the entire energy range. Moreover, the results on  $K_\alpha$  are in good agreement with the values obtained in the experiments from<sup>20,21</sup>, in contrast to a similar analysis on a conventional  $\pi$ -junction using gold<sup>30</sup>. The values of the Thouless energy inferred from the fits are both in good

agreement with the geometrical values. The solid lines in the inserts of the figure show the electron distributions, inferred from the fits, at  $V_c=0.8$  mV. For both samples the distributions are relatively rounded. In the case of the Ag device, this is mainly caused by the bath temperature of 1.4 K. In the case of the Cu sample the stronger electron-electron interaction is responsible for the extra rounding. However, the distribution is, even in this case, not quite a thermal one but still has a weak double step signature. This can be seen by the difference between the solid and the dotted line, which represents a thermal distribution with  $T_{eff} = 2.9K$ . This temperature corresponds to the effective temperature in the hot electron regime, using Eq.9 with  $V_c=0.8$  mV and  $T_{bath}=1.4K$ . Model calculations indicate that, in the case of the Cu-Nb device, a slight decrease in control channel length or measuring at a lower bath temperature would result in a distribution that is sufficiently less rounded. This would result in a transition to a  $\pi$ -state at large enough values of  $V_c$ <sup>34</sup>.

We conclude that, in the present geometry, only a Nb-Ag junction shows the transition to a  $\pi$ -junction at 1.4 K. The absolute value of the critical current and the response of the critical current to  $V_c$  are all consistent with the experimental and theoretical data available. A Nb-Cu junction does not show a transition to a  $\pi$ -junction at this temperature, but would probably do so at lower temperatures. To be able to measure at 1.4 K and higher temperatures we have fabricated controllable  $\pi$ -SQUIDS, DC SQUIDS with controllable  $\pi$ - junctions as the weak links, from Nb-Ag.

## V. CONTROLLABLE $\pi$ -SQUID

A practical realization of a controllable  $\pi$ -SQUID made of Nb-Ag is shown in Fig. 6. The fabrication procedure is identical to the fabrication of the single junctions described in Section III. The length  $L$  of the normal regions of both junctions is 1100 nm and the width  $W$  of the normal regions is 520 nm for the top junction and 220 nm for the bottom junction. The resistance of the control channels is  $8 \Omega$ , yielding a diffusion constant  $D=0.023 m^2/s$ . From  $L$  and  $D$ ,  $E_{th}$  is estimated to be  $12.6 \mu eV$  for both junctions. The area of the SQUID loop is  $12\mu m^2$ . The Thouless energy of both junctions of the SQUID are almost identical to the Thouless energy of the single junction made of silver discussed in the previous paragraph. We therefore conclude that the response of the critical current of each junction to  $V_c$  is comparable to the one presented in the top panel of Fig. 5.

### A. Experiments on a controllable SQUID

In the first experiment we measure the  $V_{SQUID} - B$  oscillations of the controllable SQUID at 1.4 K. We bias the SQUID with a low frequency AC bias current

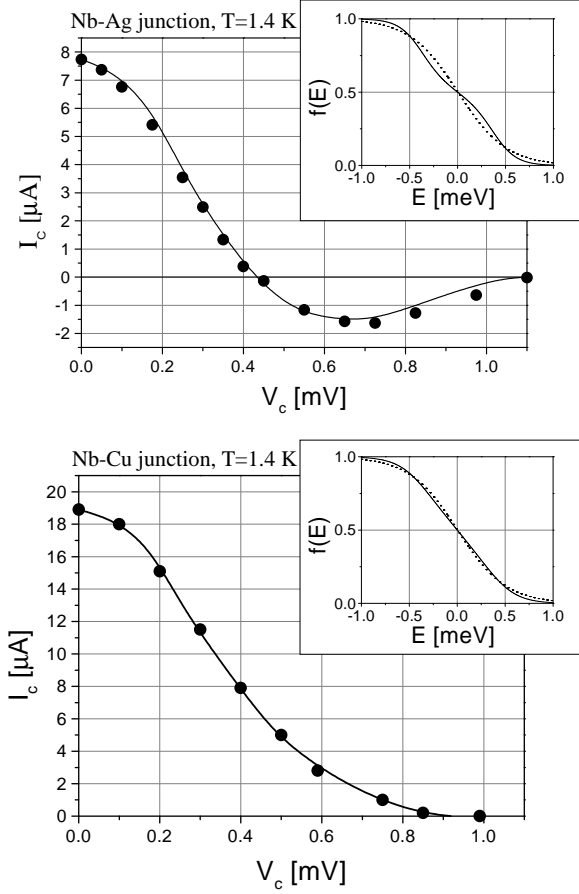


FIG. 5: Critical current of a controllable  $\pi$ -junction as shown in Fig.4, made from Cu-Nb (bottom) and Ag-Nb (top). The dots represent the data and the solid line the calculated form using Eq. 6. The solid lines in the inset show the electron distribution functions at  $V_c=0.8$  mV used in the fit. For comparison, the Fermi-Dirac distribution in the hot electron regime, with  $T_{eff} = 2.9K$ , is given by the dotted line.

( $I_{Bias}$ , 80Hz,  $4\mu A$ ) between contacts 1-2. The amplitude of the bias current is a little larger than the maximum critical current of the SQUID. The voltage over the SQUID is measured,  $V_{SQUID}$ , from contacts 1 to 2, as a function of the applied magnetic field  $B$  using a lock-in amplifier. This lock-in technique strongly reduces the noise compared to the conventional measurement method using a DC bias. Simultaneously we send a DC current through the bottom control channel and measure the resulting control voltage  $V_{c2}$ , using current sources with floating grounds. The result, using the device shown in Fig 6, is shown in Fig 7. The solid lines represents the  $V_{SQUID}$ - $B$  oscillations for increasing values of  $V_{c2}$  ( $V_{c1} = 0$ ). At first the amplitude of the oscillations decreases with increasing  $V_{c2}$  and reaches zero at  $V_{c2,critical}=0.48$  mV, indicating that the critical current of the bottom junction is equal to 0. At higher values of  $V_{c2}$  the  $V_{SQUID}$ - $B$  oscillations re-appear, with a shift

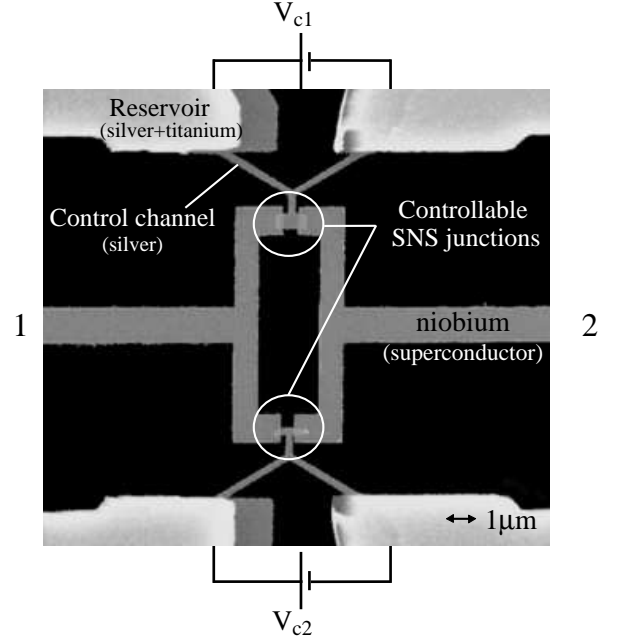


FIG. 6: Scanning electron micrograph picture of a controllable  $\pi$ -SQUID.

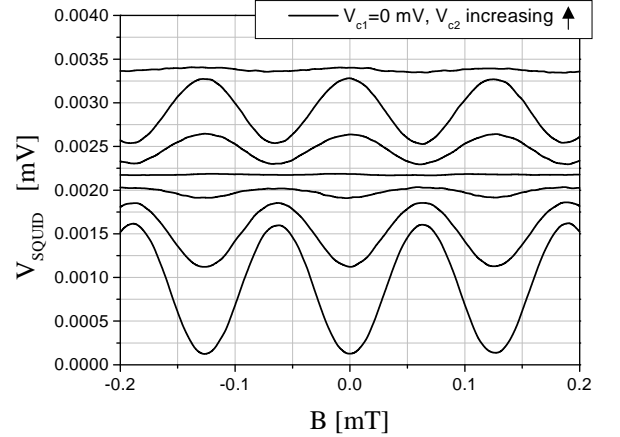


FIG. 7: The voltage over the controllable SQUID as a function of the external magnetic field  $B$  using a current bias  $I_B = 4\mu A$  (curves offset for clarity). Solid lines:  $V_{c1}=0$ ,  $V_{c2}=0.30, 0.38, 0.46, 0.48, 0.54, 0.70, 2.7$  mV (bottom to top).

$\pi$  in phase with respect to the oscillations at lower values of  $V_{c2}$ . The bottom junction and hence the SQUID, are now in the  $\pi$  state. At zero field we now measure a voltage maximum in stead of a minimum.

Using an additional current source it is possible to apply a control voltage also to the top junction. Now it is possible to add a phase of  $0, \pi$  or  $2\pi$  to the SQUID loop, as shown in Fig.8. The solid black line represent the 0-0 state, where both  $V_{c1}$  and  $V_{c2}$  are smaller than  $V_{c,critical}$ . By putting junction 1 (dotted black line in Fig.8) or junction 2 (solid grey line in the figure) in a

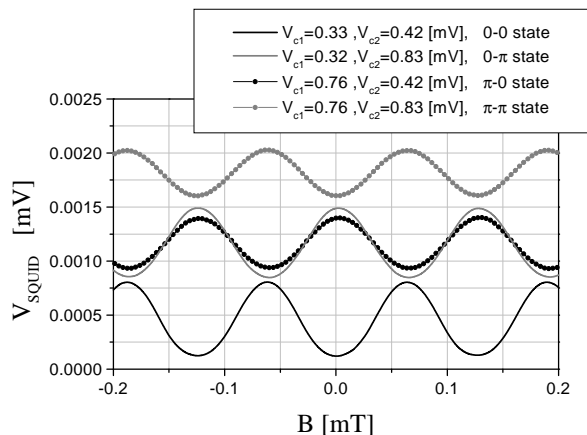


FIG. 8: The voltage over the controllable SQUID as a function of the external magnetic field  $B$  (curves offset for clarity) using both controllable junctions. The solid black line represents a 0-0 state, the solid grey line and the dotted black line represent the situation with only junction 2 or 1 in the  $\pi$ -state, respectively. The dotted grey line gives the situations for both junctions in a  $\pi$  state. Note that it has the same phase as the solid black line.

$\pi$ -state by applying a sufficiently large value of  $V_c$  we observe in both cases an identical shift of  $\pi$  in phase. By putting *both* junctions in a  $\pi$  state, as shown by the dotted grey line in Fig.8, we regain the original phase of the oscillations due to the  $2\pi$  periodicity of the macroscopic wave function around the SQUID loop. Similar measurements at 100 mK in a dilution refrigerator and at 4.2 K have shown similar results<sup>35</sup>, with however different amplitudes of the V-B oscillations due to the temperature dependence of the critical current of the Josephson junctions. These results indicate that behavior of the SQUID in the  $\pi$ -state at  $\phi_{ext} = n\phi_0$  is identical to that of a conventional SQUID at  $\phi_{ext} = (n + 1/2)\phi_0$ . This should also be valid for the screening currents in a SQUID with a sufficiently large self inductance.

## VI. DIRECT DETECTION OF THE CIRCULATING CURRENT IN A CONTROLLABLE $\pi$ -SQUID

In this Section we describe an experiment to detect the screening current in a controllable SQUID directly by placing a conventional SQUID with small self inductance inside the loop of the controllable SQUID. The device is shown in Fig.9. A controllable SQUID with a large area ( $70\mu m^2$ ) is placed upon a conventional SQUID, which we call the measurement SQUID, with an area of  $15\mu m^2$ . This SQUID has conventional SNS junctions made of gold as weak links. The two devices are electrically isolated from each other by means of 170 nm of  $Al_2O_3$ . It is important to realize that the design of the two SQUIDS is critical: The product of the screening

current  $J$  and the self inductance  $L$  of the measurement SQUID should be negligible, to prevent a disturbance of the controllable SQUID. So,  $L \cdot J \ll \phi_0$ . On the other hand the  $L \cdot J$  product of the controllable SQUID should be sufficiently large, so that the flux expelled is reasonably large. This is particularly important because the screening current is in the order of or smaller than the smallest critical current in the system. In a  $\pi$ -state the critical current of the junction is smaller than its maximum value in the normal state (see Fig.5). If these two constraints are met we expect a saw tooth behavior of the circulating current in the controllable SQUID as a function of  $\phi_{ext}$ , as shown in Fig.1. Hence we expect a saw tooth behavior of the magnetic field induced in the measurement SQUID.

The device is made on thermally oxidized silicon. In the first two steps the measurement SQUID is made using conventional e-beam lithography with a double layer of PMMA and lift-off. We start with the normal regions of the junctions, which are made of 40 nm of gold under which we use 5 nm of titanium as an adhesion layer. In the second step we DC-sputter deposit the niobium loop (60 nm) and contacts, which is done after a short *in situ* argon etching of the gold electrodes. The separation between the Nb electrode is 450 nm. To isolate the measurement SQUID we cover the entire structure, except from the contacts (outside the range of Fig. 9) with 170 nm  $Al_2O_3$  using RF sputtering. In the last two steps we fabricate a controllable SQUID on top of the small SQUID using the same fabrication procedure as described in section III.

The experiment is done at 1.4 K. The first step is to determine the maximum flux generated by the measurement SQUID. To be able to do this we measure the critical current of the measurement SQUID (at  $\phi_{ext} = 1/2\phi_0$  and 0) while suppressing the flux generated by the controllable SQUID. The latter is achieved by means of applying a control voltage exactly equal to the critical control voltage to the bottom junction of the controllable SQUID. This results in a total suppression of the critical current of this junction, i.e.  $J=0$ . Hence we obtain the critical current of the measurement SQUID at  $\phi_{ext} = 0$  of  $4.2\mu A$  and  $200\text{ nA}$  at  $\phi_{ext} = 0.5\phi_0$ . The maximum flux generated by the screening current in the measurement SQUID can be estimated from these measurements using Eq. 1, 2 and 3 to be less than  $0.05\phi_0$ , assuming the worst case scenario of exactly identical critical currents for both junctions<sup>36</sup>. This indicates that the measurement SQUID does not influence the controllable SQUID. In the next step we estimate the self inductance of the controllable SQUID using the data given in Table III.

The critical currents of the bottom and top junctions,  $I_{c2}$  and  $I_{c1}$  respectively, are measured by applying precisely the critical control voltage to one junction (reducing its critical current to 0) and measure the transport critical current through the SQUID. From these values we can estimate  $L=65\text{ pH}$ . This value of  $L$  would result

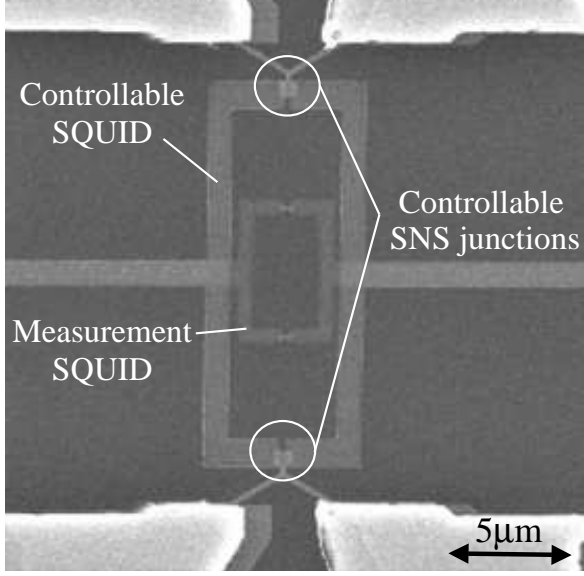


FIG. 9: Scanning electron microscope of a device that consists of a controllable  $\pi$ -SQUID with a smaller conventional DC SQUID (measurement SQUID) placed inside its loop. The two devices are electrically isolated by means of 170 nm of  $\text{Al}_2\text{O}_3$ . The flux expelled from the big controllable SQUID is detected using the measurement SQUID.

TABLE III: Parameters of the controllable SQUID to estimate the self inductance taken at 1.4 K.  $I_{c,MAX} = I_c$  at  $\phi_{ext} = 0$  and  $I_{c,MIN} = I_c$  at  $\phi_{ext} = \frac{1}{2}\phi_0$ .  $I_{c2}$  ( $I_{c1}$ ) is the critical current of the bottom (top) junction in Fig.9.

$I_{c,MAX}$ [ $\mu\text{A}$ ]	$I_{c,MIN}$ [ $\mu\text{A}$ ]	$I_{cB}$ [ $\mu\text{A}$ ]	$I_{cT}$ [ $\mu\text{A}$ ]
88	76	74	14

in a maximum expelled flux at 1.4 K, if no control voltages are applied to the junctions, of  $0.34 \phi_0$  associated with  $J = 11 \mu\text{A}$ .

In the experiment we measure the  $V_{SQUID} - B$  oscillations of the *measurement* SQUID using a suitable low frequency AC bias current. This is done for different values of  $V_{c2}$  on the *controllable* SQUID. A representative result is shown in Fig. 10. The grey line indicates the situation where  $V_{c2} = V_{c2,critical} = 0.745 \text{ mV}$ . In this case  $I_{c2} = J = 0$ . The result is an (almost) sinusoidal voltage with a period of 0.134 mT, which represents  $\phi_0$  for the small measurement SQUID. The black line shows the situation where  $V_{c2} < V_{c2,critical} = 0.62 \text{ mV}$ . In this case periodic deviations from the grey line are observed associated with the screening current in controllable SQUID. The periodicity of the deviations is given by  $B(\phi_{0,controllableSQUID}) \equiv B(\Phi_0) = 0.029 \text{ mT}$ . The ratio  $\frac{B(\Phi_0)}{B(\phi_0)} = \frac{0.029}{0.134} \approx \frac{15}{70}$  which is the ratio of the areas of the two SQUIDS. It is this difference in area and hence in periodicity, that makes it possible to obtain information over the circulating current in the large controllable

SQUID over several fluxquanta within less than half a fluxquantum in the measurement SQUID. To make the result more clear we can extract the magnetic field induced in the measurement SQUID by the screening current in the controllable SQUID from this data: We subtract the grey curve from the black one, and multiply this difference by  $(\frac{\partial V}{\partial B})^{-1}$ , which is obtained by numerically differentiating the grey curve. Obviously the data around  $0, \frac{1}{2}, 1, 1\frac{1}{2} \dots \phi_0$  are not obtainable because the sensitivity of the measurement SQUID is zero at these points. We perform this analysis on a set of data at different values of  $V_{cB}$ . The result is shown in Fig.11 for 2 different values of  $V_{c2}$ <sup>37</sup>. We observe that the black line, which is the same measurement as shown in Fig. 10 ( $V_{c2} > V_{c2,critical} = 0.62 \text{ mV}$ ), is a saw tooth function around integer flux, consistent with the behavior of the screening current in a SQUID with a relatively large self inductance, as shown in Fig.1c. The grey line, for which  $V_{c2} > V_{c2,critical} = 1.08 \text{ mV}$ , shows the exact same behavior, with however a shift of half a flux quantum. In this case a screening current flows, in either the clockwise or counterclockwise direction, at integer external flux.

These measurements indicate that it is possible, around an integer flux quantum, to switch between a conventional state without a screening current and a state with a (bistable) screening current by applying  $V_{c2} > V_{c2,critical}$ . This is illustrated more clearly by the data in Fig.12. In this figure we show a measurement of the magnetic field induced in the bottom SQUID as a function of the  $V_{c2}$  (in stead of  $\phi_{ext}$ ) for two different values of the applied external flux around -1 fluxquantum. At  $V_{c2} < V_{c2,critical}$  the field induced in the measurement SQUID is a horizontal line close to 0, indicating that hardly any flux is expelled from the controllable SQUID. Hence no screening current flows around the

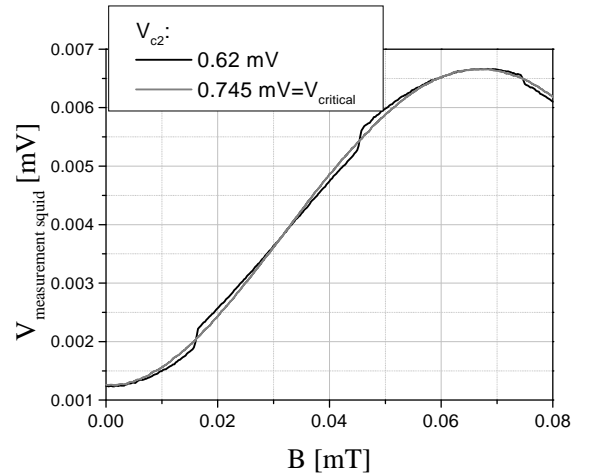


FIG. 10: Voltage measured over the *measurement* SQUID as a function of magnetic field for two values of the control voltage on the bottom junction of the *controllable* SQUID.  $V_{c2} = 0.745$  represents the critical control voltage.

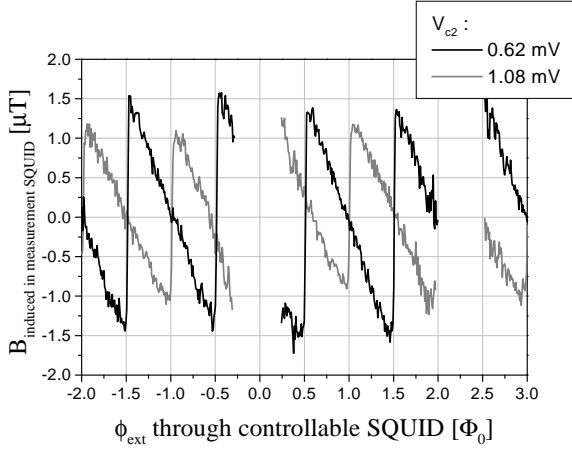


FIG. 11: The magnetic field induced in the *measurement* SQUID by the flux generated by the screening current in the *controllable* SQUID as a function of the external flux given in units of  $\Phi_0$ , representing one flux quantum through the controllable SQUID. The data is given for two different values of the control voltage over the bottom junction of the controllable SQUID.

loop of the controllable SQUID as expected. However, if  $V_{c2} > V_{c2,critical}$  we see an increase (or decrease) of the induced magnetic field, associated with the screening current caused by the introduction of an extra phase factor of  $\pi$  ( $-\pi$ ) in the SQUID loop. The sign of the signal depends on the exact value of the external flux. At  $\phi_{ext} = -1.1\phi_0$  (black line), the induced field is negative, consistent with Fig.11. This clearly indicates that it is possible to switch from a state with no current running around the SQUID loop to a non zero current state. The small a-symmetries in the figure are caused by the magnetic field associated with the current flowing in the control channel of the bottom junction.

## VII. CONCLUSIONS

We have demonstrated that in a controllable  $\pi$ -SQUID a screening current can be generated without the application of an external magnetic field by putting one con-

trollable  $\pi$ -junction of the SQUID into a  $\pi$ -state. At a measurement temperature of 1.4 K and with the present geometry, only a Nb-Ag controllable  $\pi$  junction shows the transition to a  $\pi$  state, in contrast with a Nb-Cu device. We have shown that this difference is caused by the difference in electron-electron interaction strength between Ag and Cu, consistent with direct measurements of this quantity on similar diffusive wires using tunnel junction spectroscopy<sup>20,21</sup>. The possibility of adding an extra phase of  $\pi$  to the SQUID loop is demonstrated not only by the screening current, but also by the fact that the  $V_{SQUID} - B$  oscillations can be shifted by a phase factor of  $\pi$  or  $2\pi$ , depending whether one or two controllable

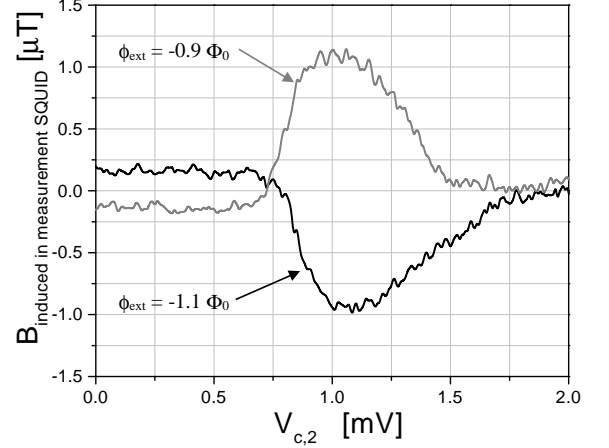


FIG. 12: The magnetic field induced in the measurement SQUID by the flux generated by the screening current in the controllable SQUID as a function of the control voltage applied over the bottom control channel of the controllable SQUID. The data is shown for 2 values of the external flux  $\Phi$  through the *controllable* SQUID around -1 fluxquantum.

junctions are put on a  $\pi$ -state.

We gratefully acknowledge H. Pothier and F.K. Wilhelm for discussions and for making their computer programs available to us. This work was supported by the Nederlandse Organisatie voor Wetenschappelijk Onderzoek (NWO) through the Stichting voor Fundamenteel Onderzoek der Materie (FOM).

<sup>1</sup> A.F. Volkov, Phys. Rev. Lett. **74**, 4730 (1995).

<sup>2</sup> A.F. Volkov, H. Takayanagi, Phys. Rev. B. **56**, 11184 (1997).

<sup>3</sup> F.K. Wilhelm, G. Schön, A.D. Zaikin, Phys. Rev. Lett. **81**, 1682 (1998).

<sup>4</sup> S.-K Yip, Phys. Rev. B **58**, 5803 (1998).

<sup>5</sup> B.J.van Wees, K.-M.H.Lenssen and C.J.P.M.Harmans Phys. Rev. B Rap. Com. **44**, 470 1991

<sup>6</sup> A.F. Morpurgo, T.M. Klapwijk and B.J. van Wees, Appl. Phys. Lett. **72**, 966-968 (1998)

<sup>7</sup> K. Neurohr, Th. Schäpers, J. Malindretos, S. Lachenmann, A.I. Braginski, H. Lüth, M. Behet, G. Borghs, A.A. Golubov, Phys. Rev. B **59**, 11197 (1999).

<sup>8</sup> J. Kutchinsky, R. Taboryski, C.B. Sorensen, J.B. Hansen and P.E. Lindelof, Phys. Rev. Let. **83**, 4856 (1999)

<sup>9</sup> J.J.A. Baselmans, A.F. Morpurgo, B.J van Wees, T.M. Klapwijk, Nature **397**, 43 (1999).

<sup>10</sup> R.Shaikhaidarov, A.F.Volkov, H.Takayanagi, V.T.Petrashov, P.Delsing, Phys.Rev. B **62**, R14649 (2000)

- <sup>11</sup> C.C. Tsuei, J.R. Kirtley, C.C. Chi, Lock See Yu-Jahnes, A. Gupta, T. Shaw, J.Z. Sun, M.B. Ketchen, Phys. Rev. Lett. **73**, 593 (1994); A. Mathai, Y. Gim, R.C. Black, A. Amar, F.C. Wellstood, Phys. Rev. Lett. **74**, 4523 (1995)
- <sup>12</sup> D.J. van Harlingen, Rev. Mod. Phys. **67**, 515 (1995)
- <sup>13</sup> V.V. Ryazanov, V.A. Oboznov, A. Yu. Rusanov, A.V. Veretennikov, A.A. Golubov, J.Aarts, Phys. Rev. Lett **86**, 2427 (2001)
- <sup>14</sup> A system with a weak link between two Superfluid <sup>3</sup>He reservoirs shows a stable state around a phase  $\phi=0$  and a meta stable state around  $\phi = \pi$  with respect to the mass current through the weak link. See S.Backhaus, S. Pereverzev, R.W. Simmonds, A. Loshak, J.C. Davids and R.E Packard, Nature **392**, 687 (1998)
- <sup>15</sup> J.Clarke in *SQUID sensors, Fundamentals, Fabrication, and Applications*, edited by H. Weinstock, NATO ASI Series 329, Dordrecht, 1-62 (1996).
- <sup>16</sup> M. Cryot and D. Pavuna, in *Introduction to superconductivity and high-T-c materials*, World Scientific, Singapore, (1992).
- <sup>17</sup> M. Tinkam, in *Introduction to Superconductivity*, McGraw-Hill, Singapore, (1996).
- <sup>18</sup> We have used the fact that the critical current generally equals the supercurrent if the phase difference is  $\pi/2$ . This is not fully correct, but only leads to minor changes in the calculated curves<sup>3,4</sup>.
- <sup>19</sup> P. Dubos, H. Courtois, B. Pannetier, F.K Wilhelm, A.D. Zaikin, and G. Schön, Phys. Rev. B, **63**, 064502 (2001)
- <sup>20</sup> H. Pothier, S.Guéron, N.O. Birge, D. Estève, M.H. Devoret, Phys. Rev. Lett. **79**, 3490 (1997).
- <sup>21</sup> F. Pierre, H. Pothier, D. Estève, M.H. Devoret, J. of low Temp. Phys. **118**, 437 (2000).
- <sup>22</sup> A.B. Gougam, F. Pierre, H. Pothier, D. Estève, Norman O. Birge, M.H. Devoret, J. of Low Temp. Phys. **118**, 447 (2000).
- <sup>23</sup> F. Pierre, H. Pothier, D. Estève, M.H. Devoret, A.B. Gougam and Norman O. Birge in *Kondo effect and dephasing in low dimensional metallic systems*, eds. Venkat Chandrasekhar, Chris Van Haesendonck, and Alfred Zawadowski (Kluwer Academic Publishers, Dordrecht, 2001). e-print: arXiv: cond-mat/0012038 (2000).
- <sup>24</sup> B.L. Altshuler, A.G. Aronov, Zh. Eksp. Teor. Fiz **75**, 1610 (1978) [Sov. Phys. JETP **48**, 812 (1978)]
- <sup>25</sup> B.L. Altshuler A.G. Aronov in *Electron-Electron interactions in Disordered Systems*, eds. A.L. Efros, M. Pollak, Elsevier Science publishers B.V. (North-Holland, Amsterdam 1985)
- <sup>26</sup> F. Pierre in *Interactions electron-electron dans les fils mesoscopiques (electron-electron interactions in mesoscopic wires)* Ph.D. Thesis CEA-SACLAY (2000)
- <sup>27</sup> F. C. Wellstood, C. Urbina, J. Clarke, Phys. Rev. B **49**, 5942 (1994).
- <sup>28</sup> M. Henny, S. Oberholzer, C. Strunk, C. Schönenberger, Phys. Rev. B **59**, 2871 (1999)
- <sup>29</sup> The dominant thermal resistance in our system is the one associated with electron heat diffusion from the control channel into the reservoirs<sup>28</sup>. We estimated the electron diffusion heating parameter  $b$  valid for our samples at 1.4 K,  $b \leq 0.05 \text{ k/mV}$ . The calculated effective electron temperature in the reservoirs  $T_{eff} = \sqrt{T_{bath}^2 + bV_c^2}$ , yields a negligible electron heating in the range of  $V_c$  used in the experiments  $0 \leq V_c \leq 1.2 \text{ mV}$ .
- <sup>30</sup> J.J.A. Baselmans, B.J. van Wees, T.M. Klapwijk, Phys. Rev. B **63**, 094504 (2000)
- <sup>31</sup> The use of a Ge suspended mask, which is more stable than the presented PMMA mask, is not suitable because the electron beam exposure of the large area reservoirs has to be done using relatively high beam currents ( nA), to come to a reasonable exposure time. This results in stress in the PMMA-MA-Ge-PMMA resist, causing the germanium to crack.
- <sup>32</sup> D. Esteve et al. in *Mesoscopic electron transport: NATO ASI series E*, vol. 345, 469 (eds. Sohn, L.L. et al.)(Kluwer Academic, Dordrecht/Boston/London, 1997)
- <sup>33</sup> B.J. van Wees, H. Takayanagi, in *Mesoscopic electron transport: NATO ASI series E*, vol. 345, 375 (eds. Sohn, L.L. et al.)(Kluwer Academic, Dordrecht/Boston/London, 1997)
- <sup>34</sup> We calculated  $I_c$  as a function of  $\tau_D$  with identical parameters and found that at  $\tau_D=2\text{ns}$  the transition to a  $\pi$ -state would occur at 1.4K. At  $T < 1\text{K}$  the transition would even occur with the sample as it is.
- <sup>35</sup> J.J.A. Baselmans, B.J. van Wees, T.M. Klapwijk, Appl. Phys. Lett **79**, 2940 (2001)
- <sup>36</sup> The self inductance would be 45 pH in the case of identical junctions. However, the difference in transport critical current between  $\phi = 0$  and  $\phi = \phi_0/2$  can also be attributed to small difference in critical currents between the junctions. This assumption gives  $L=0$  and a difference in critical current of 10 percent. We must conclude that  $L \leq 45\text{pH}$  for the measurement SQUID.
- <sup>37</sup> In Fig. 11 we have corrected for a slight horizontal and vertical shift between the curves that is caused by the current associated with  $V_{c2}$  flowing through the control channel. The flux associated with this current causes a horizontal shift between the curves due to the coupling in the controllable SQUID, identical to the one in Fig.7 and a vertical shift due to the coupling into the measurement SQUID.